UNIVERSITY OF LEEDS

Robust Converter Control Design under Time-Delay Uncertainty

David Rodriguez Flores*, Uros Markovic*, Petros Aristidou§, Gabriela Hug*

* EEH - Power Systems Laboratory, ETH Zurich, Physikstrasse 3, 8092 Zurich, Switzerland
§ School of Electronic and Electrical Engineering, University of Leeds, Leeds LS2 9JT, UK
Emails: roddavid@student.ethz.ch, {markovic, hug}@eeh.ee.ethz.ch, p.aristidou@leeds.ac.uk

Abstract—**This paper deals with the converter control design under time delay uncertainty in power systems with high share of converter-based generation. Two approaches for time delay modeling are proposed using linear fractional transformations and linear parameter-varying systems, respectively. Subsequently, two output-feedback synthesis methods are implemented based on $\mathcal{H}_\infty$ control theory, and formulated using linear matrix inequalities: (i) a norm-bounded parametric $\mathcal{H}_\infty$ controller; and (ii) a gain-scheduled $\mathcal{H}_\infty$ control. These robust control principles are then employed to improve the performance of Voltage Source Converters (VSCs) under varying measurement delays. Three novel control strategies are proposed in order to redesign the conventional inner control loop and improve converter performance when dealing with measurement uncertainty. Finally, the controllers are integrated into a state-of-the-art VSC model and compared using time-domain simulations.**

Index Terms—**low-inertia systems, time delay, voltage source converter (VSC), linear fractional transformation (LFT), linear parameter-varying (LPV) system, robust stability, $\mathcal{H}_\infty$ control**

I. INTRODUCTION

Conventional synchronous machines are being gradually replaced by renewable energy sources, interfaced to the grid through power electronic devices. The loss of traditional generators comes along with the decrease in total rotational inertia of the system, thus affecting the system stability margins [1]. This problem has so far been dealt with through advanced converter AC-side control schemes, such as the virtual synchronous machine [2], machine matching [3] and dispacthable virtual oscillator control [4]. However, all of the proposed approaches involve local signal measurements, which are often subjective to time delays.

The subject of local time delay is often ignored in the area of power system control due to large time constants of the associated machine regulators. Nonetheless, with shorter timescales, characteristic of low-inertia systems, the impact of local converter measurements might play an important role in the overall system stability. Different approaches for time-delay modeling have previously been investigated in [5], concluding that the Padé approximation and Chebyshev discretization scheme prevail as the most efficient methods. However, the focus was set solely on constant measurement delays with no uncertainty. A probabilistic approach for modelling the delays

as a random variable and employing Monte Carlo simulations was used in [6], while [7] proposes a use of Lyapunov functions for deriving the delay-dependent stability criteria. The studies in [8] and [9] employ classical $\mathcal{H}_\infty$ methods to deal with fixed delays, and [10] suggests a parameter-dependent $\mathcal{H}_\infty$ gain-scheduling for delays within a certain tolerance. Other approaches in the literature consider a use of Smith predictors [11], adaptive control schemes [12] and lead-lag compensators [13]. Nonetheless, all aforementioned studies focus on conventional power systems and the underlying delays in wide-area measurements. While some concerns regarding the impact of local converter delays in low-inertia systems have already been raised in [14], it was done for a simplistic system without considering the delay uncertainty.

The contribution of this work is three-fold. First, we propose two ways of modelling the delay uncertainty and incorporating it into the Robust Control (RC) design. Moreover, two different output-feedback $\mathcal{H}_\infty$ controllers are employed, each using a different delay uncertainty model, and compared under different measurement delay conditions. Finally, three novel RC strategies for redesigning the conventional Voltage Source Converter (VSC) control scheme are introduced, and analyzed using $\mathcal{H}_\infty$-based techniques.

The remainder of the paper is structured as follows. In Section II the necessary RC principles along with the modelling of uncertain time delays are presented. The state-of-the-art converter control scheme and the novel robust controllers are described in Section III. Section IV showcases the detailed time-domain simulation results of the proposed control designs and compares their respective performances. Finally, Section V draws the main conclusions and discusses the outlook of the study.

II. RC PRINCIPLES UNDER TIME-DELAY UNCERTAINTY

A. Time Delay Modelling

We assume a real parametric uncertainty, and model the time delays in two different ways: (i) as a Linear Fractional Transformation (LFT); and (ii) as a Linear Parameter-Varying (LPV) system. In both cases the delays are modelled as exponential functions $F(s) = e^{-\tau_d s}$ in the Laplace domain and are approximated using a first-order Padé approximation of the form:

$$F(s) = e^{-\tau_d s} \approx \frac{1 - \frac{1}{2}\tau_d s}{1 + \frac{1}{2}\tau_d s}, \tag{1}$$
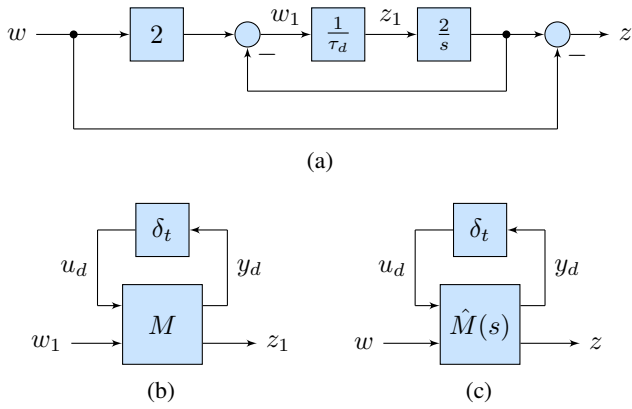
(a)

(b)   (c)

Fig. 1: Equivalent representation of the delay function $F(s)$: (a) control block scheme; (b) LFT formulation of the delay block τ_d^{-1}; (c) LFT formulation of the delay function $F(s)$.

1) Time Delay as an LFT:

The relation between the original signal w and its delayed counterpart z can be expressed as

$$z = F(s)w \longmapsto z = -w + \frac{2}{\tau_d s}(w - z) \qquad (2)$$

which corresponds to the block diagram in Fig. 1a. The time delay parameter τ_d changes within a 1-dimensional polytope $[\underline{\tau}_d, \overline{\tau}_d]$. By defining $a = \frac{1}{2}(\underline{\tau}_d + \overline{\tau}_d)$, $b = \frac{1}{2}(\overline{\tau}_d - \underline{\tau}_d)$ and $\delta_t \in [-1, 1]$, one can formulate such polytope as $\tau_d = a + b\delta_t$. Therefore, the time-delay block τ_d^{-1} can be represented as an upper LFT of the form $F_u(M, \delta_t)$ shown in Fig. 1b, with

$$M = \begin{bmatrix} -ba^{-1} & a^{-1} \\ -ba^{-1} & a^{-1} \end{bmatrix} \qquad (3)$$

Substituting $F_u(M, \delta_t)$ in Fig. 1a and performing a set of mathematical transformations yields the final LFT form depicted in Fig. 1c, equivalent to the initial delay function $F(s)$, where

$$\hat{M} = \begin{bmatrix} \hat{M}_{11} & \hat{M}_{12} \\ \hat{M}_{21} & \hat{M}_{22} \end{bmatrix} = \frac{1}{-as + 2b} \begin{bmatrix} as + b & -2 \\ 2bs & -s \end{bmatrix} \qquad (4)$$

2) Time Delay as an LPV function:

Let us consider a delayed-input system without the controller. Based on the Padé approximation from (1), the following state-space representation of the delay can be derived:

$$\dot{x}_d = -\frac{2}{\tau_d}x_d + \frac{4}{\tau_d}u_d \qquad (5)$$
$$y_d = x_d - u_d$$

where u_d and y_d are the delayed input and output of the system, and x_d is the internal delay state. Substituting q for τ_d^{-1} yields

$$\begin{bmatrix} A_d(q) & B_d(q) \\ C_d(q) & D_d(q) \end{bmatrix} = \begin{bmatrix} -2q & 4q \\ 1 & -1 \end{bmatrix} \qquad (6)$$

The system in (6) can be rewritten as an affine parameter-dependent system, with the state-space matrices of the delay described as affine functions of the parameter q:

$$\begin{bmatrix} A_d(q) & B_d(q) \\ C_d(q) & D_d(q) \end{bmatrix} = \begin{bmatrix} A_{d_0} + qA_{d_1} & B_{d_0} + qB_{d_1} \\ C_{d_0} + qC_{d_1} & D_{d_0} + qD_{d_1} \end{bmatrix} \qquad (7)$$
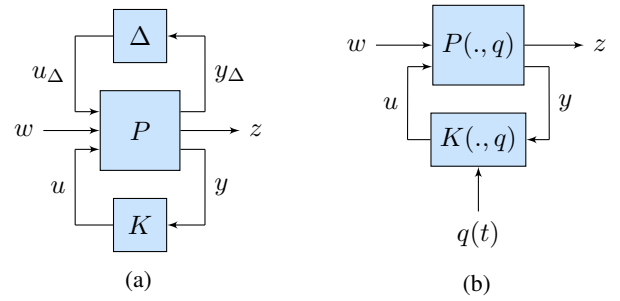

(a)   (b)

Fig. 2: General control plant: (a) LFT general plant. (b) LPV general plant.

B. $\mathcal{H}_\infty$ Control Design

This section elaborates on the principles of $\mathcal{H}_\infty$ control. For the generic linear system described in (8), the $\mathcal{H}_\infty$ norm is the maximum gain of the transfer function from exogenous inputs w to exogenous outputs z over all frequencies and input directions [15]. When designing $\mathcal{H}_\infty$ controllers the system is rearranged into a so-called general control form illustrated in Fig. 2, where $P(s)$, $K(s)$ and Δ are the transfer functions of the plant, controller and uncertainty respectively; the uncertainty transfer function is not needed for the purposes of LPV system design. Therefore, without considering the uncertainty, let $P(s)$ be of the following form:

$$\dot{x} = Ax + B_1 w + B_2 u$$
$$z = C_1 x + D_{11} w + D_{12} u \qquad (8)$$
$$y = C_2 x + D_{21} w + D_{22} u$$

with u being the control input and y the control measurement. The $\mathcal{H}_\infty$ problem involves designing a controller that stabilizes the closed loop system and results in

$$\left\| T_{wz}(s) \right\|_\infty < \gamma \qquad (9)$$

for a given γ. Depending on the employed control synthesis method, the closed-loop system will also guarantee a degree of robustness against model uncertainty.

In order to shape the sensitivity function $S(s)$ and complementary sensitivity function $K(s)S(s)$ of the closed-loop system, and achieve the desired robustness and performance targets, a mixed-sensitivity $\mathcal{H}_\infty$ design depicted in Fig. 3 is often used, which minimizes

$$\left\| \begin{bmatrix} W_1(s)S(s) \\ W_2 K(s)S(s) \end{bmatrix} \right\|_\infty \qquad (10)$$

The weight transfer function $W_1(s)$ is usually a low-pass filter with the purpose of improving the output disturbance rejection or reference tracking, whereas $W_2(s)$ is a high-pass filter used for minimizing the control effort at high frequencies [15]. The mixed-sensitivity design is then solved by computing the augmented plant $P(s)$ from the open-loop transfer function $G(s)$ and aforementioned weighting functions.

For control analysis, the robustness of the system is calculated through the concepts of robust and quadratic stability [16]. The former guarantees stability for the whole
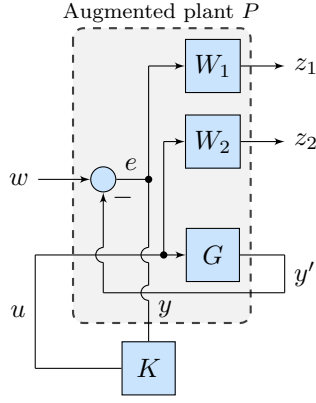
Fig. 3: Mixed sensitivity $\mathcal{H}_\infty$ design.

uncertainty range and can be determined either through the structural singular value μ for LFT systems [15], or via a parameter-dependent Lyapunov function in the case of an LPV system [17]. Quadratic stability, on the other hand, is a fundamentally stronger concept of stability since it guarantees robust stability, as well as the resilience to arbitrary fast parameter changes [18]. However, it is also more conservative due to a single Lyapunov function being used for the whole uncertainty range.

C. Control Synthesis Methods

Two control synthesis methods are used, one for LFT modeling and another for LPV modeling. Both methods are defined using Linear Matrix Inequalities (LMIs) and are based on the concept of quadratic stability [18], [19]. Additional constraints are specified to place the poles of the closed-loop system in a specific region of the left-half plane in order to ensure the prescribed damping ratio requirements [20]. Both control synthesis problems are solved in MATLAB using the Yalmip interface [21] and SeDuMi/SDPT3 solvers [22], [23].

1) $\mathcal{H}_\infty$ Control for Norm-Bounded Parametric Systems: We aim to solve the $\mathcal{H}_\infty$ performance problem of the form:

$$\|H_{wz}\|_\infty < 1 \ , \forall \, \|\Delta\|_2 \leq 1 \tag{11}$$

which is equivalent to the robust stability of the closed-loop system with a virtual norm-bounded uncertainty $\Delta_P(s)(\|\Delta_P\|_\infty \leq 1)$ inserted between the disturbance d and the error e [18]. Therefore, the overall uncertainty becomes $diag(\Delta, \Delta_P)$. A scaling matrix $L = diag(I, \sqrt{\ell}I)$ can be subsequently introduced to reduce the conservatism of the small-gain method as follows:

$$\left\| L^{1/2} H_{zw} L^{-1/2} \right\|_\infty < \gamma \tag{12}$$

where L is permutable with $diag(\Delta, \Delta_P)$.

The scaled $\mathcal{H}_\infty$ problem is solved if and only if there exist matrices $X > 0$, $Y > 0$, and L, J satisfying the following

conditions:

$$\begin{bmatrix} N_X^T & 0 \\ 0 & I_{n_w} \end{bmatrix} \begin{bmatrix} AX + XA^T & XC_1^T & B_1 \\ C_1X & -\gamma J & D_{11} \\ B_1^T & D_{11}^T & -\gamma L \end{bmatrix} \begin{bmatrix} N_X & 0 \\ 0 & I_{n_w} \end{bmatrix} < 0$$

$$\begin{bmatrix} N_Y^T & 0 \\ 0 & I_{n_z} \end{bmatrix} \begin{bmatrix} YA + A^TY & YB_1 & C_1^T \\ B_1^TY & -\gamma L & D_{11}^T \\ C_1 & D_{11} & -\gamma J \end{bmatrix} \begin{bmatrix} N_Y & 0 \\ 0 & I_{n_z} \end{bmatrix} < 0 \tag{13}$$

$$\begin{bmatrix} X & I \\ I & Y \end{bmatrix} \geq 0$$

$$LJ = I$$

The last equality $LJ = I$ is not convex, but the problem can be solved using the *K-L iteration method* proposed in [18].

2) Gain-Scheduled (GS) $\mathcal{H}_\infty$ Control for LPV Systems: This problem seeks a controller of the form:

$$\dot{x}_k = A_k(q)x_k + B_k(q)u_k \tag{14}$$

$$y_k = C_k(q)x_k + D_k(q)u_k \tag{15}$$

When the parameter vector $q(t)$ takes values in a box $\mathcal{B} \in \mathbb{R}^n$ with $N = 2^n$ corners, then the system $G(q)$ is confined within a matrix polytope defined by vertices $G(\theta_i)$. Given the convex decomposition

$$q = \sum_{i=1}^N \alpha_i \theta_i \tag{16}$$

the controller state space can be written as

$$\begin{bmatrix} A_k(q) & B_k(q) \\ C_k(q) & D_k(q) \end{bmatrix} = \sum_{i=1}^N \alpha_i \begin{bmatrix} A_k(\theta_i) & B_k(\theta_i) \\ C_k(\theta_i) & D_k(\theta_i) \end{bmatrix} \tag{17}$$

Subsequently, the controller operating point q is found through convex interpolation of the LTI vertex controllers:

$$K_i = \begin{bmatrix} A_k(\theta_i) & B_k(\theta_i) \\ C_k(\theta_i) & D_k(\theta_i) \end{bmatrix}$$

The gain-scheduling problem can be thus solved by solving the following LMI problem for symmetric matrices X and Y:

$$\begin{bmatrix} N_{12} & 0 \\ 0 & I \end{bmatrix}^T \begin{bmatrix} A(\theta_i)X + XA^T(\theta_i) & XC_1^T(\theta_i) & B_1(\theta_i) \\ C_1(\theta_i) & -\gamma I & D_{11}(\theta_i) \\ B_1^T & D_{11}^T(\theta_i) & -\gamma I \end{bmatrix} \begin{bmatrix} N_{12} & 0 \\ 0 & I \end{bmatrix} < 0$$

$$\begin{bmatrix} N_{21} & 0 \\ 0 & I \end{bmatrix} \begin{bmatrix} A^T(\theta_i)Y + YA & YB_1(\theta_i) & C_1^T(\theta_i) \\ B_1^T(\theta_i)Y & -\gamma I & D_{11}^T(\theta_i) \\ C_1(\theta_i) & D_{11}(\theta_i) & -\gamma I \end{bmatrix} \begin{bmatrix} N_{21} & 0 \\ 0 & I \end{bmatrix} < 0 \tag{18}$$

$$\begin{bmatrix} X & I \\ I & Y \end{bmatrix} \geq 0$$

with N_{12} and N_{21} denoting the bases of the null spaces of (B_2^T, D_{12}^T) and (C_2, D_{21}) respectively. The optimal controller K is derived from X and Y.

III. VSC CONTROL DESIGN

A. VSC Control Scheme

We consider a state-of-the-art VSC control scheme previously described in [24], where the outer control loop consists of droop-based active and reactive power controllers providing the output voltage angle and magnitude reference by adjusting the predefined setpoints (x^*) according to a measured power imbalance. Subsequently, the reference voltage vector signal
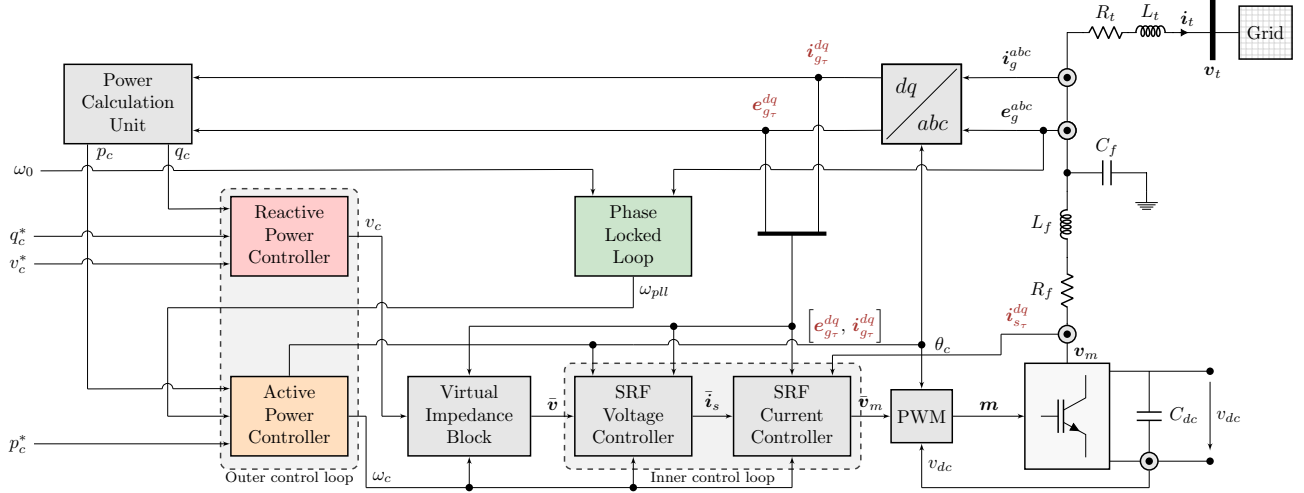
Fig. 4: General configuration of the implemented VSC control structure. The delayed measurements are denoted in red.

$(v_c \angle \theta_c)$ is passed through a virtual impedance block, as well as the inner control loop consisting of cascaded voltage and current controllers. The output is combined with the DC-side voltage in order to generate the modulation signal m. In order to detect the system frequency at the connection terminal, a synchronization unit in the form of a phased-locked loop is included in the model. Furthermore, the time delays are imposed onto the local measurement signals (e_g, i_g, i_s), denoted with a subscript τ in Fig. 4. Since the measurements are obtained from a single device, we assume the same time delay for all signals. The complete mathematical model consists of 15 states, with inclusion of the filter current and voltage dynamics, and is implemented in a rotating (dq)-frame and per unit. More details on the overall converter control structure, employed parametrization, potential operation modes and respective transient properties can be found in [24].

B. Robust Control Design

The vulnerability of the system to measurement delays is first evaluated through small-signal stability for a wide range of time delays. The eigenvalue spectrum illustrated in Fig. 5 indicates a critical delay of $\hat{\tau}_d \approx 314\,\mu s$, and suggests the presence of 4 critical modes. According to the participation factor analysis, the states with the highest participation in those modes are the filter current and voltage (i_s, e_g), with the former having the highest impact. Hence, the inner control loop can be considered the main cause of instability.

The traditional inner control design consists of a cascade of PI controllers and feed-forward loops, as follows:

$$\bar{\boldsymbol{i}}_s = \left(K_p^v + \frac{K_i^v}{s} \right)(\bar{\boldsymbol{v}} - \boldsymbol{e}_g) + j x_f \boldsymbol{e}_g + K_f^i \boldsymbol{i}_g \quad (19)$$

$$\bar{\boldsymbol{v}}_m^{(0)} = \left(K_p^i + \frac{K_i^i}{s} \right)\Delta\boldsymbol{i}_{s_\tau} + j x_f \boldsymbol{i}_{s_\tau} + K_f^v \boldsymbol{e}_{g_\tau} \quad (20)$$

where $\Delta\boldsymbol{i}_{s_\tau} = \bar{\boldsymbol{i}}_s - \boldsymbol{i}_{s_\tau}$, the subscripts p, i and f denote the respective proportional, integral and feed-forward gains, and the superscripts v and i refer to the voltage and current control.
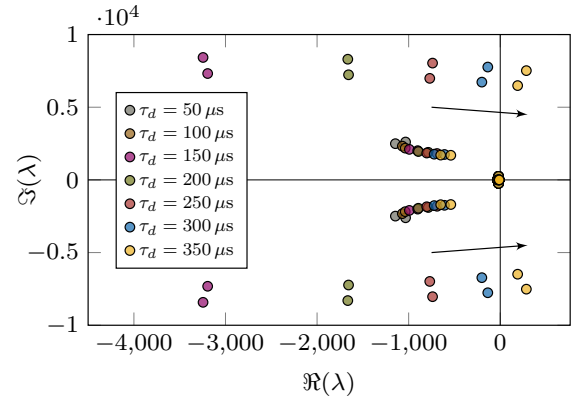

Fig. 5: Root loci spectrum around the imaginary axis computed using the Padé approximation.

In order to improve the converter performance under measurement delay, we propose three novel control strategies:

$$\bar{\boldsymbol{v}}_m^{(1)} = \left(K_p^i + \frac{K_i^i}{s} \right)\Delta\boldsymbol{i}_{s_\tau} + j x_f \boldsymbol{i}_{s_\tau} + K_f^v \boldsymbol{e}_{g_\tau} - \mathcal{K}_1(\Delta\boldsymbol{e}_{g_\tau})$$

$$\bar{\boldsymbol{v}}_m^{(2)} = \left(K_p^i + \frac{K_i^i}{s} \right)\Delta\boldsymbol{i}_{g_\tau} + j x_f \boldsymbol{i}_{g_\tau} + K_f^v \boldsymbol{e}_{g_\tau} - \mathcal{K}_2(\Delta\boldsymbol{e}_{g_\tau})$$

$$\bar{\boldsymbol{v}}_m^{(3)} = \mathcal{K}_3(\bar{\boldsymbol{v}} - \boldsymbol{e}_{g_\tau}) \quad (21)$$

The first two approaches depicted in Fig. 6a consist of adding an additional damping term $\mathcal{K}_{1,2}$ to the current control based on the deviation of the voltage across the filter capacitor from its nominal value $(\Delta\boldsymbol{e}_{g_\tau})$. The latter design also uses different current input measurement, replacing the switching current $\boldsymbol{i}_{s_\tau}$ with the grid current input $\boldsymbol{i}_{g_\tau}$ in order to reduce the control sensitivity to time delay. On the other hand, motivated by the fact that the states associated with the inner loop have the highest participation in critical modes, the third configuration completely redefines this control block and designs a uniform robust controller $\mathcal{K}_3$ that explicitly computes the modulation voltage setpoint of the converter. Such concept also eliminates
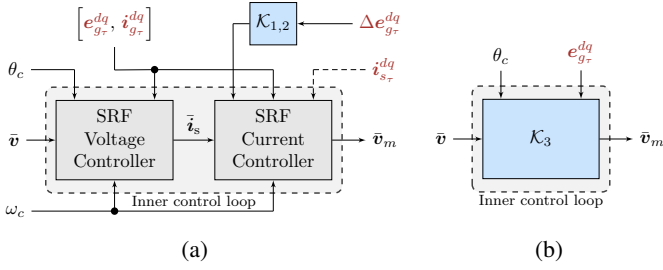
Fig. 6: Control design strategies: (a) robust active damping control ($\mathcal{K}_1, \mathcal{K}_2$); (b) uniform robust inner control ($\mathcal{K}_3$).

the need for any current measurement input, as described in Fig. 6b, thus providing a lower controller order.

Two $\mathcal{H}_\infty$ output feedback controllers are implemented for each design: an LFT norm-bounded controller and a GS controller, previously described in Section II-C. The weighting transfer functions used in the mixed-sensitivity design of $\mathcal{K}_1$ and $\mathcal{K}_2$ are: $W_1(s) = \frac{0.5s+500}{s+5}$, $W_2(s) = 1$. Since the controller $\mathcal{K}_3$ tracks the voltage output of the converter, the weights are chosen such that a good integral control performance in time domain is achieved. The bandwidth of the controller is therefore set to 1000 rad/s, resulting in the following weighting functions: $W_1(s) = \frac{0.5s+1000}{s+0.1}$, $W_2(s) = 1$.

IV. RESULTS

An overview of the stability performance obtained from the proposed control designs is presented in Table I. We can observe that the range of time delays for which the robust and quadratic stability are guaranteed, as well as the order of the controllers, vary significantly between different control approaches. As described previously in Section II, the emphasis is put on quadratic stability, as it allows for arbitrarily fast variation of measurement delays. Understandably, $\mathcal{K}_3$ has the lowest order due to removal of the current measurements from the control input. It also provides a drastically larger stability range, both under LFT and GS implementation. This is a consequence of its conceptually superior design, which eliminates a majority of the state feedback sensitive to time delays. Moreover, the GS approach appears to be the more robust of the two, with the respective critical delay $\hat{\tau}_d$ reaching millisecond range.

We now investigate the converter response to a 10% step increase in active power setpoint, and evaluate its reference tracking capability under different measurement delay properties. For this purpose, detailed time-domain simulations in

TABLE I: Stability performance of different control designs.

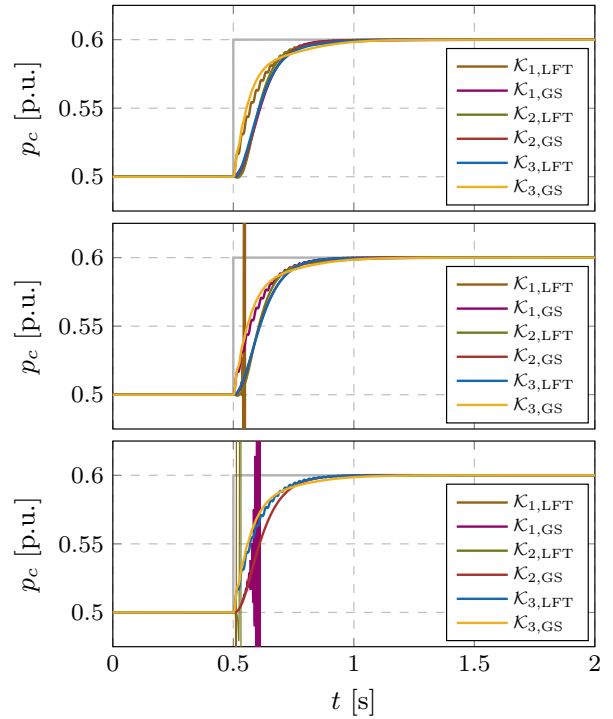| Control	Order	QS Range	RS Range
$\mathcal{K}_{1,\text{LFT}}$	21	$[0-370]\ \mu$s	$[0-420]\ \mu$s
$\mathcal{K}_{1,\text{GS}}$	21	$[0-750]\ \mu$s	$[0-750]\ \mu$s
$\mathcal{K}_{2,\text{LFT}}$	19	$[0-400]\ \mu$s	$[0-660]\ \mu$s
$\mathcal{K}_{2,\text{GS}}$	19	$[0-2]$ ms	$[0-2]$ ms
$\mathcal{K}_{3,\text{LFT}}$	15	$[0-900]\ \mu$s	$[0-1]$ ms
$\mathcal{K}_{3,\text{GS}}$	15	$[0-20]$ ms	$[0-50]$ ms

Fig. 7: Response to a step-change in active power setpoint under constant time delay for different inner control designs: (i) $\tau_d = 150\ \mu$s; (ii) $\tau_d = 500\ \mu$s; (iii) $\tau_d = 1$ ms;.

MATLAB Simulink have been used. A focus is first set on constant delays in a range of $[150-1000]\ \mu$s and the results are presented in Fig. 7. Under a reasonably small delay of $150\ \mu$s all controllers achieve good performance, with controller $\mathcal{K}_{3,\text{GS}}$ having the best overall response due to a combination of its reduced system order and gain scheduling design. Nonetheless, such level of delay could be withstood by a conventional inner control, which is not the case in the next two scenarios. For $\tau_d \in [500, 1000]\ \mu$s we observe that certain control designs are unstable, which can be justified by their insufficient robust stability range in Table I. More precisely, $\mathcal{K}_{1,\text{LFT}}$ has a critical delay threshold below $500\ \mu$s, whereas $\mathcal{K}_{1,\text{GS}}$ and $\mathcal{K}_{2,\text{LFT}}$ cannot withstand a 1 ms measurement delay.

Accounting for time delay variability, a quadratic stability aspect becomes more relevant, as it ensures resilience to fast changes in the delay signal. Therefore, we consider a delay varying as a sinusoidal function of the form $\tau_d = T_d |\sin(\omega t)|$, with $T_d = 1$ ms. The converter power response illustrated in Fig. 8 indicates that only the controllers with an acceptable quadratic stability range can tolerate such an oscillatory delay nature. As a result, the LFT designs of $\mathcal{K}_1$ and $\mathcal{K}_2$ underperform whenever τ_d goes drastically above $370\ \mu$s and $400\ \mu$s, respectively. A similar characteristic is noticeable for $\mathcal{K}_{3,\text{LFT}}$, with $\hat{\tau}_d = 900\ \mu$s being slightly below the delay peak. Interestingly, the GS configuration reacts differently when the delays exceed the permissible range, manifested through stable, but highly oscillatory behavior of $\mathcal{K}_{1,\text{GS}}$. Finally, $\mathcal{K}_{2,\text{GS}}$ and $\mathcal{K}_{3,\text{GS}}$ face no instability issues due to very broad quadratic
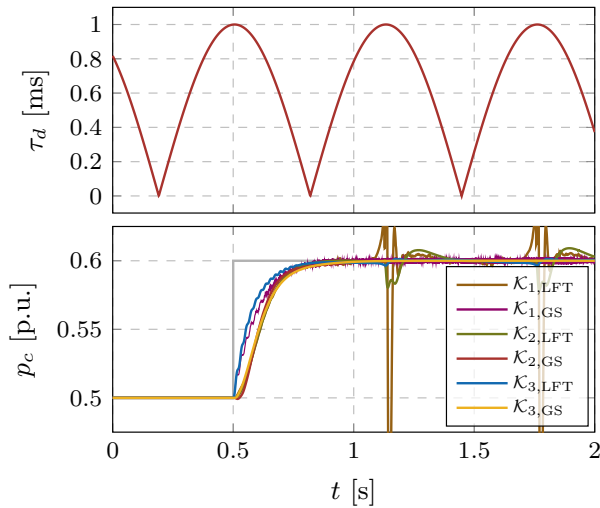
Fig. 8: Response to a step-change in active power setpoint under varying time delay for different inner control designs: (i) varying time delay signal; (ii) converter power output.

stability ranges.

It can be concluded that the $\mathcal{K}_3$ concept clearly shows the best performance, independent of the control synthesis method. It completely replaces the inner control loop, reduces the overall control order and ensures excellent robustness to any type of measurement delay. On the other hand, the $\mathcal{K}_1$ and $\mathcal{K}_2$ configurations have an inherent disadvantage of adding an extra controller to the existing system and increasing complexity. Furthermore, $\mathcal{K}_1$ achieves only a minor improvement to the original design, whereas $\mathcal{K}_2$, although significantly better, is still suboptimal compared to the uniform structure of $\mathcal{K}_3$.

V. CONCLUSION

In this paper, the robust control design under time delay uncertainty in power systems with a high share of converter-based generation is investigated. Two ways of time delay modeling are presented, and subsequently used for developing two output-feedback synthesis methods based on $\mathcal{H}_\infty$ control theory. In order to improve the resilience of VSCs to varying delays in local measurement, three novel control strategies are proposed and combined with each of the two synthesis methods. A redesign of the conventional inner control loop is suggested, which improves converter performance when dealing with measurement uncertainty. It was found that the uniform controller performs the best and guarantees quadratic stability for a wide range of time delays. Furthermore, the gain-scheduling synthesis appeared to be the more practical approach of the two. Future work will focus on large-scale systems, as well as the impact of signal delay in wide-area measurements involved in centralized power system control schemes.

REFERENCES

[1] A. Ulbig, T. S. Borsche, and G. Andersson, "Impact of low rotational inertia on power system stability and operation," *IFAC Proceedings Volumes*, vol. 47, no. 3, pp. 7290 – 7297, 2014.

[2] J. Driesen and K. Visscher, "Virtual synchronous generators," in *2008 IEEE Power and Energy Society General Meeting - Conversion and Delivery of Electrical Energy in the 21st Century*, July 2008.

[3] C. Arghir, T. Jouini, and F. Dörfler, "Grid-forming control for power converters based on matching of synchronous machines," *Automatica*, vol. 95, pp. 273 – 282, 2018.

[4] M. Colombino, D. Groß, J.-S. Brouillon, and F. Dörfler, "Global phase and magnitude synchronization of coupled oscillators with application to the control of grid-forming power inverters," *arXiv preprint arXiv:1710.00694*, 2017.

[5] F. Milano, "Small-signal stability analysis of large power systems with inclusion of multiple delays," *IEEE Transactions on Power Systems*, vol. 31, no. 4, pp. 3257–3266, 2016.

[6] S. Ayasun and C. O. Nwankpa, "Probability of small-signal stability of power systems in the presence of communication delays," in *Electrical and Electronics Engineering, 2009. ELECO 2009. International Conference on*. IEEE, 2009, pp. I–70.

[7] T. Li, M. Wu, and Y. He, "Lyapunov-Krasovskii functional based power system stability analysis in environment of wams," *Journal of Central South University of Technology*, vol. 17, no. 4, pp. 801–806, 2010.

[8] D. Ke, C. Chung, and Y. Xue, "An eigenstructure-based performance index and its application to control design for damping inter-area oscillations in power systems," *IEEE Transactions on Power Systems*, vol. 26, no. 4, pp. 2371–2380, 2011.

[9] R. Shah, N. Mithulananthan, K. Y. Lee *et al.*, "Large-scale pv plant with a robust controller considering power oscillation damping," *IEEE Transactions on Energy Conversion*, vol. 28, no. 1, pp. 106–116, 2013.

[10] H. Wu, K. S. Tsakalis, and G. T. Heydt, "Evaluation of time delay effects to wide-area power system stabilizer design," *IEEE Transactions on Power Systems*, vol. 19, no. 4, pp. 1935–1941, Nov 2004.

[11] T. Zabaiou, L.-A. Dessaint, F.-A. Okou, and R. Grondin, "Wide-area coordinating control of svcs and synchronous generators with signal transmission delay compensation," in *Power and Energy Society General Meeting, 2010 IEEE*. IEEE, 2010, pp. 1–9.

[12] B. Chaudhuri, R. Majumder, and B. C. Pal, "Wide-area measurement-based stabilizing control of power system considering signal transmission delay," *IEEE Transactions on Power Systems*, vol. 19, no. 4, pp. 1971–1979, 2004.

[13] P. Zhang, D. Yang, K. Chan, and G. Cai, "Adaptive wide-area damping control scheme with stochastic subspace identification and signal time delay compensation," *IET generation, transmission & distribution*, vol. 6, no. 9, pp. 844–852, 2012.

[14] U. Markovic, P. Aristidou, and G. Hug, "Stability performance of power electronic deviceswith time delays," in *2017 IEEE Manchester PowerTech*. IEEE, 2017.

[15] S. Skogestad and I. Postlethwaite, *Multivariable feedback control: analysis and design*. Wiley New York, 2007, vol. 2.

[16] B. Barmish, "Stabilization of uncertain systems via linear control," *IEEE Transactions on Automatic Control*, vol. 28, no. 8, pp. 848–850, 1983.

[17] W. Haddad and D. Bernstein, "Parameter-dependent lyapunov functions, constant real parameter uncertainty, and the popov criterion in robust analysis and synthesis. 1," in *Decision and Control, 1991., Proceedings of the 30th IEEE Conference on*. IEEE, 1991, pp. 2274–2279.

[18] K.-Z. Liu and Y. Yao, *Robust control: theory and applications*. John Wiley & Sons, 2016.

[19] P. Apkarian and P. Gahinet, "A convex characterization of gain-scheduled $\mathcal{H}_\infty$ controllers," *IEEE Transactions on Automatic Control*, vol. 40, no. 5, pp. 853–864, May 1995.

[20] M. Chilali, P. Gahinet, and P. Apkarian, "Robust pole placement in lmi regions," *IEEE transactions on Automatic Control*, vol. 44, no. 12, pp. 2257–2270, 1999.

[21] J. Lofberg, "Yalmip: A toolbox for modeling and optimization in matlab," in *Computer Aided Control Systems Design, 2004 IEEE International Symposium on*. IEEE, 2004, pp. 284–289.

[22] J. F. Sturm, "Using sedumi 1.02, a matlab toolbox for optimization over symmetric cones," *Optimization methods and software*, vol. 11, no. 1-4, pp. 625–653, 1999.

[23] K.-C. Toh, M. J. Todd, and R. H. Tütüncü, "Sdpt3a matlab software package for semidefinite programming, version 1.3," *Optimization methods and software*, vol. 11, no. 1-4, pp. 545–581, 1999.

[24] U. Markovic, J. Vorwerk, P. Aristidou, and G. Hug, "Stability analysis of converter control modes in low-inertia power systems," in *2018 IEEE Innovative Smart Grid Technologies - Europe (ISGT-Europe)*, Oct 2018.